EARTH SURFACE PROCESSES AND LANDFORMS
Earth Surf. Process. Landforms **45**, 1469–1482 (2020)

Published online 5 February 2020 in Wiley Online Library
(wileyonlinelibrary.com) DOI: 10.1002/esp.4818

The impact of internal waves on upper continental slopes: insights from the Mozambican margin (southwest Indian Ocean)

Elda Miramontes[1,2]*† Gwenael Jouet,[2] Estelle Thereau,[2] Miguel Bruno,[3] Pierrick Penven,[4] Charline Guerin,[2] Pascal Le Roy,[1] Laurence Droz,[1] Stephan J. Jorry,[2] F. Javier Hernández-Molina,[5] Antoine Thiéblemont,[5,6] Ricardo Silva Jacinto[2] and Antonio Cattaneo[2]
[1] UMR6538, CNRS-UBO, IUEM, Laboratoire Géosciences Océan, Plouzané, France
[2] IFREMER, Unité Géosciences Marines, Plouzané, France
[3] CACYTMAR, Universidad de Cádiz, Puerto Real, Cádiz, Spain
[4] UMR 6523 CNRS, IFREMER, IRD, UBO, Laboratoire d'Océanographie Physique et Spatiale, Plouzané, France
[5] Department of Earth Sciences, Royal Holloway, University of London, Egham, Surrey, UK
[6] TOTAL, R&D Frontier Exploration Programme, Pau, France

Received 15 July 2019; Revised 20 December 2019; Accepted 29 December 2019

*Correspondence to: Elda Miramontes, UMR6538, CNRS-UBO, IUEM, Laboratoire Géosciences Océan, 29280 Plouzané, France. E-mail: emiramon@uni-bremen.de
†Present Address: Faculty of Geosciences, University of Bremen, 28359 Bremen, Germany or MARUM-Centre for Marine Environmental Sciences, University of Bremen, 28359 Bremen, Germany.

ESPL
Earth Surface Processes and Landforms

ABSTRACT: Evidences of sedimentation affected by oceanic circulation, such as nepheloid layers and contourites are often observed along continental slopes. However, the oceanographic processes controlling sedimentation along continental margins remain poorly understood. Multibeam bathymetry and high-resolution seismic reflection data revealed a contourite depositional system in the Mozambican upper continental slope composed of a contourite terrace (a surface with a gentle seaward slope dominated by erosion) and a plastered drift (a convex-shape sedimentary deposit). A continuous alongslope channel and a field of sand dunes (mainly migrating upslope), formed during Holocene, were identified in the contourite terrace at the present seafloor. Seismic reflection data of the water column show internal waves and boluses propagating in the pycnocline near the upper slope. The channel and the dunes are probably the result of the interaction of the observed internal waves with the seafloor under two different conditions. The alongslope channel is located in a zone where intense barotropic tidal currents may arrest internal solitary waves, generating a hydraulic jump and focused erosion. However, upslope migrating dunes may be formed by bottom currents induced by internal solitary waves of elevation propagating landwards in the pycnocline. These small-scale sedimentary features generated by internal waves are superimposed on large-scale contouritic deposits, such as plastered drifts and contourite terraces, which are related to geostrophic currents. These findings provide new insights into the oceanographic processes that control sedimentation along continental margins that will help interpretation of palaeoceanographic conditions from the sedimentary record. © 2020 The Authors. Earth Surface Processes and Landforms published by John Wiley & Sons Ltd.

KEYWORDS: contourite; sediment drift; bedform; sedimentary processes; tide; internal solitary waves; bottom currents

Introduction

Contourite depositional systems are sedimentary systems that contain depositional (contourite drifts) and erosional features (moats, contourite channels, furrows, etc.) generated by oceanic currents that can be found on continental margins worldwide (Hernández-Molina et *al.*, 2008; Rebesco et *al.*, 2014). They are formed by a variety of oceanographic processes that occur at different temporal and spatial scales, such as geostrophic currents, eddies, overflows, dense shelf-water cascading, barotropic and baroclinic tidal currents or internal solitary waves (ISWs) (Rebesco et *al.*, 2014; Hernández-Molina et *al.*, 2016a). Despite the ubiquity of contourites, little is known about how the different oceanographic processes affect continental slopes due to the paucity of direct observations and modelling studies in deep-sea settings (Hunter et *al.*, 2007; de Lavergne et *al.*, 2016; Hernández-Molina et *al.*, 2016b).

The presence of nepheloid layers (i.e. layers of water above the seafloor containing significant amounts of suspended sediment) on upper continental slopes has often been related to the elevated bottom shear stresses generated by internal waves (Cacchione and Drake, 1986; Puig et *al.*, 2004). Internal waves

[Correction added on 5 May 2020, after first online publication: the address for correspondence has been updated in this version. The first author's present addresses have also been indicated.]

may affect continental slopes at different spatial scales: (i) They may determine the average slope angle of continental margins (about 2°–4°), which is an order of magnitude lower than the internal friction angle of marine sediment (Cacchione et *al.*, 2002); (ii) Internal waves may also be at the origin of dune fields, as observed for instance in the South China Sea (Ma et *al.*, 2016) and in the Messinian Strait (Droghei et *al.*, 2016), or sediment waves, as suggested in the western (Ribó et *al.*, 2016) and eastern Mediterranean Sea (Reiche et *al.*, 2018).

The internal tide energy generated on the slope and shelf break may radiate away in two different ways: (i) horizontally in the form of interface internal waves at tidal frequency (internal baroclinic tides); or (ii) as internal tidal beams into the stratified water column (da Silva et *al.*, 2009; Lamb, 2014). The continental slope of Mozambique is a zone of intense internal tide generation (Baines, 1982; Manders et *al.*, 2004; da Silva et *al.*, 2009; Magalhaes et *al.*, 2014) that could affect sedimentation on this margin.

This study aims to improve the identification and characterization of the oceanographic processes that control the formation of sediment bodies and erosional features along continental margins in order to better constrain how sediment is transported from the continent to the deep sea, and to provide arguments for the reconstruction of past oceanographic conditions based on sediment architecture. The main objectives of this study are to: (i) characterize the morphology, lithology and age of the contourite depositional system in the upper continental slope of the Mozambican margin; and (ii) identify the main oceanographic processes that may be at the origin of the observed erosional and depositional features. In this study, we focus on the upper continental slope of the Mozambican margin, in an area located in the Sofala Bank offshore the Zambezi delta (Figure 1).

Regional Setting

Geological setting

Sediment transfer from land to ocean basins is strongly controlled by sediment supply and sea-level fluctuations, especially in areas with extended continental shelves such as the Mozambican margin (van der Lubbe et *al.*, 2014; Wiles et *al.*, 2017). The primary sediment source of the Mozambican margin is the Zambezi River, which with a catchment area of 1.4×10^6 km^2 (Walford et *al.*, 2005) is one of the largest river systems of eastern Africa (Fekete et *al.*, 1999). During sea-level low-stands, the Zambezi River supplied sediment directly to the shelf edge and the continental slope (Schulz et *al.*, 2011). In contrast, at present and during past sea-level high-stands, sediments are dispersed towards the northeast along the coast and then southwards on the upper continental slope (Figure 1C; Beiersdorf et *al.*, 1980; Schulz et *al.*, 2011; Wiles et *al.*, 2017).

Sedimentation in the Mozambique Channel is controlled by bottom currents at all depths, from the Mozambican continental shelf (Flemming and Kudrass, 2018) to the deep part of the basin (Kolla et *al.*, 1980; Breitzke et *al.*, 2017; Wiles et *al.*, 2017; Miramontes et *al.*, 2019a). The southern part of the Mozambican continental slope (south of 21°S) is dominated by a contourite depositional system that is composed of a series of contourite terraces and plastered drifts at different water depths, from the shelf edge down to 2200 m below sea level (b.s.l.) (Thiéblemont et *al.*, 2019). Plastered drifts are characterized by a convex shape, with higher sediment accumulation in the centre of the deposit (Faugères and Stow, 2008). In their proximal part, they are commonly associated with contourite terraces, which are large, broad and gently tilting seaward (< 2°) surfaces dominated by erosional features (Hernández-Molina et *al.*, 2009, 2017; Preu et *al.*, 2013; Thiéblemont et *al.*, 2019). North of 21°S, the margin is more dominated by gravity-driven sedimentary processes, with common submarine-landslide scars and deposits, and turbidite channels (Fierens et *al.*, 2019; Thiéblemont et *al.*, 2019). In this area, only the shallowest terrace and plastered drift (~300 m b.s.l.), which are the focus of the present study, are present on the upper continental slope (Thiéblemont et *al.*, 2019).

Oceanographic setting

Currents in the Mozambique Channel are very complex and intense, with surface currents up to 2 m s^{-1} (Ternon et *al.*, 2014)

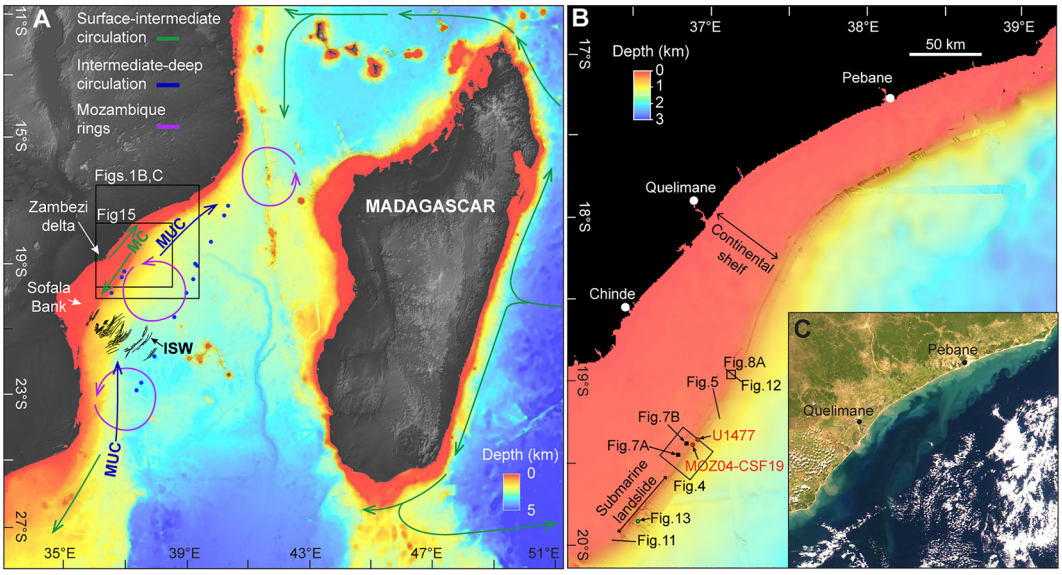

Figure 1. (A) Bathymetric map of the Mozambique Channel, showing the main ocean currents. The blue dots indicate the location of the CTD (conductivity, temperature and depth) data used in Figure 2. The black lines represent the internal solitary waves (ISWs) identified by da Silva *et al.* (2009) from Envisat advanced synthetic aperture radar (ASAR) imagery. MC: Mozambique Current; MUC: Mozambique Undercurrent. (B) Zoom of the bathymetric map showing the study area. (C) NASA Worldview satellite image of 21 June 2016, showing how river plumes are deflected towards the north by alongshore currents and sediment in suspension is carried from the northern part towards the south by offshore currents. [Colour figure can be viewed at wileyonlinelibrary.com]

and bottom currents in the deep basin up to 0.5 m s^{-1} (Miramontes et *al.*, 2019a). Surface currents along the Mozambican margin are part of the greater Agulhas Current system, which extends from north Madagascar to South Africa (Lutjeharms, 2006). The Agulhas Current is the strongest western boundary current in the southern hemisphere, and results in an important exchange of heat and salt between the Indian and Atlantic Oceans (Gordon, 1986; Weijer et *al.*, 1999). Surface and intermediate circulation along the Mozambican continental slope mainly comprises a southward-bound, western boundary current [Mozambique Current (MC)] (DiMarco et *al.*, 2002; Quartly et *al.*, 2013; Flemming and Kudrass, 2018) and large anticyclonic eddies (≥ 300 km diameter, Mozambique rings) that migrate southwards and can affect the entire water column (de Ruijter et *al.*, 2002; Lutjeharms et *al.*, 2012; Halo et *al.*, 2014) (Figure 1A).

The surface waters in the Mozambique Channel are composed of tropical surface water (TSW) (upper 100–150 m) and subtropical surface water (STSW) (from 100 to 150 m b.s.l. to about 300 m b.s.l.) (Figure 2; Ullgren et *al.*, 2012). The TSW is formed in the tropics by surface warming and excess precipitation (Ullgren et *al.*, 2012), while the STSW is formed in the area from 25°S to 35°S due to greater evaporation than precipitation, and is characterized by a subsurface salinity maximum when it is present below the TSW (Figure 2; Wyrtki, 1973). The south Indian central water (SICW) forms the permanent thermocline, and is formed by sunken surface water (You, 1997). The SICW is characterized by a linear potential temperature–salinity relationship between 300 and 600 m b.s.l. (Figure 2; Ullgren et *al.*, 2012). Intermediate waters (> 600 m b.s.l.) in the Mozambique Channel are composed of Red Sea water (RSW) that flows into the Mozambique Channel from the north, and Antarctic intermediate water (AAIW) that enters from the south as part of the Mozambique undercurrent (MUC) (Figure 1; Ullgren et *al.*, 2012).

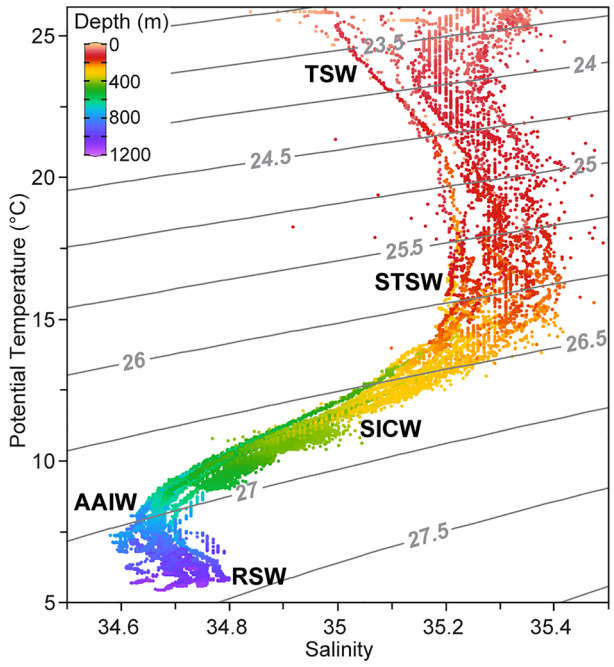

Figure 2. Potential temperature-salinity diagram showing the main water masses that affect the upper slope of the Mozambican margin generated with Ocean Data View (Schlitzer, 2018). The grey lines represent the potential density anomaly (kg m^{-3}). TSW: tropical surface water; STSW: subtropical surface water; SICW: south Indian central water; AAIW: Antarctic intermediate water; RSW: Red Sea water. See Figure 1A for CTD location. [Colour figure can be viewed at wileyonlinelibrary.com]

The Mozambican slope is a hot spot for the generation of internal tides and ISWs (da Silva et *al.*, 2009). ISWs observed in this area travel offshore (Figure 1A), and are generated at the shelf break and at about 80 km seawards of the shelf break due to the interaction of the internal tidal rays with the thermocline (da Silva et *al.*, 2009). Despite the evidences of internal waves in this area, their impact on sedimentation and on shaping the seafloor was not clearly demonstrated in previous studies.

Material and Methods

The regional bathymetry used for this study (Figure 1) is GEBCO bathymetry (GEBCO_08, version 2010-09-27, http://www.gebco.net), with a 30 arc-second resolution. The main data shown in the present study were collected during the PAMELA-MOZ04 survey (2015, R/V *Pourquoi pas?*; Jouet and Deville, 2015). The multibeam bathymetry and the co-registered backscatter intensity were acquired with the Kongsberg EM710 and Kongsberg EM122 systems. The horizontal resolution of the multibeam bathymetry is 20 m in the upper slope (up to about 700 m b.s.l.) and 40 m in the deeper areas. The multibeam bathymetry acquired with the EM710 system was re-gridded independently in the areas of the dune field and the channel to increase the resolution to 3 and 5 m, respectively. These high-resolution bathymetry maps were used to measure dune and channel morphologies. In order to improve the visualization of the dunes on the slope, we calculated the average plane (mean bathymetric surface) every 100 m and we subtracted the depth of the average plane from the original multibeam bathymetry at a horizontal resolution of 3 m. The resulting differential map represents the dune crests as positive values (above the mean bathymetric surface) and the dune troughs as negative values (below the mean bathymetry surface).

A satellite image of 21 June 2016 was obtained from the NASA Worldview application (https://worldview.earthdata.nasa.gov), using the Visible Infrared Imaging Radiometer Suite (VIIRS) corrected reflectance imagery.

The seismic data consists of 72-channel high-resolution mini GI-gun seismic reflection profiles (50–250 Hz) that imaged the water column and the seafloor, and sub-bottom profiler (SBP) data (1800–5300 Hz). In order to remove noise and artefacts in the water column in the vicinity of the seafloor, singular value decomposition was applied to normal moveout stacked data in the water column before migration. Seismic data were acquired during a period of spring tides (Figure 3), when barotropic tidal currents are stronger, intensifying the generation of internal waves.

One Calypso piston core (MOZ04-CSF19, 9.12 m long) was collected on the upper continental slope (Figure 1B). The core was dated using radiocarbon analyses on bulk planktonic foraminifera performed at Beta Analytic Laboratories. Radiocarbon ages were calibrated using the Marine13 calibration curve (Reimer et *al.*, 2013).

Hydrographic data [conductivity, temperature and depth (CTD) profiles] were obtained from the World Ocean Database 2013 (WOD13; https://www.nodc.noaa.gov/OC5/WOD13/) and the Coriolis Database (http://www.coriolis.eu.org/), and used to identify the water masses present near the Mozambican slope. In addition, we also collected one expendable bathythermograph (XBT) profile and one XCTD profile on the Mozambican upper slope during the PAMELA-MOZ04 survey. The characteristic angles for the semi-diurnal internal tides (c) were calculated using the XCTD data acquired on the upper slope, resampled every 5 m, following

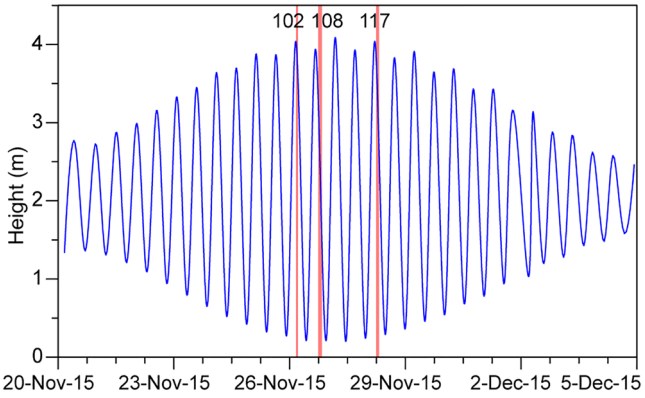

Figure 3. Predicted tide height at Chinde, Mozambique (see Figure 1B for location). The red bands correspond to the periods of acquisition of the seismic profiles MOZ04-HR-102, MOZ04-HR-108 and MOZ04-HR-117. They were all collected during spring tides, profile 102 was collected on average during high tide, 108 2.5 hours after high tide and 117 1 hour after high tide. [Colour figure can be viewed at wileyonlinelibrary.com]

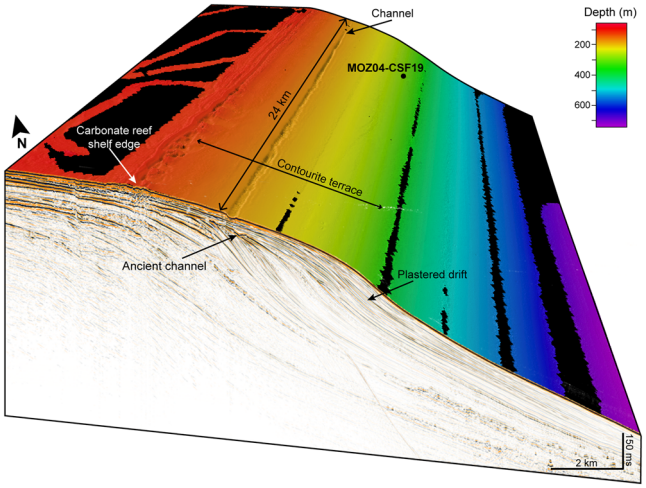

Figure 4. Three-dimensional block composed of multibeam bathymetry and multi-channel high-resolution seismic reflection profile MOZ04-HR-114, showing the main sedimentary features observed in the upper slope and the location of core MOZ04-CSF19. See Figure 1B for location. [Colour figure can be viewed at wileyonlinelibrary.com]

the method of Cacchione *et al.* (2002). The angle c is given by:

$$c = \pm\left(\frac{\sigma^2 - f^2}{N^2 - \sigma^2}\right)^{1/2}, \quad (1)$$

where σ is the internal wave frequency, which is 0.081 cycles per hour (cph) for internal tides at semi-diurnal tidal frequency; f is the local inertial frequency at a latitude φ (19.5°S and 19°S), where $f = \sin(\varphi)/12$ cph; and N is the local Brunt–Väisälä (or buoyancy) frequency, which is calculated as:

$$N^2 = \frac{-g}{\rho}\frac{\partial \rho}{\partial z}, \quad (2)$$

The slope criticality (i.e. how tidal beams are reflected from the slope) is analysed according to ratio between the seafloor slope angle (γ) and the natural internal wave propagation angle (c): (i) transmissive or subcritical conditions when $\gamma < c$; (ii) critical or near critical conditions when $\gamma \approx c$; and (iii) reflective or supercritical conditions when $\gamma < c$ (Cacchione et *al.*, 2002).

Results

Contourite depositional system along the upper continental slope

The upper slope of the Mozambican margin off the Zambezi delta consists of a plastered drift and a contourite terrace, which separates the plastered drift from the edge of the continental shelf (Figure 4). The plastered drift shows a convex morphology, with a steep slope (up to 5°–6°) in its lower part at 300–400 m b.s.l. The contourite terrace comprises the proximal domain of the plastered drift (located at 120–300 m b.s.l.), which is characterized by a gentle slope (mostly below 2° dipping seaward) and by the presence of truncated reflections, suggesting that the terrace was affected by erosional processes or is still undergoing erosion. The plastered drift is characterized by continuous convex reflections, indicating that it is a main depositional area (Figures 4 and 5).

The seafloor along the outer part of the contourite terrace (at 315 m b.s.l.) (Figure 4) is covered by straight to slightly sinuous sandy ripples. The troughs of the ripples seem to contain coarser sediment (Figure 6A). This area was sampled by sediment core MOZ04-CSF19 that shows marked changes in grain size, characterized by a coarser layer at the core top (Figure 6B). The bottom of the core is mainly composed of muddy deposits with a mean grain size of 30 µm. The upper 2 m of the sediment core are mainly composed of a coarsening-up sand layer, with sand volumetric concentration increasing from 33% to 89% and mean grain sizes from 71 µm to 243 µm (Figure 6B).

Heavy minerals such as zircon can be accumulated due to winnowing under intense bottom currents (e.g. Bahr et *al.*, 2014). Calcium/titanium (Ca/Ti) ratio is typically used as a proxy for comparing marine and terrigenous sediment input, due to the higher content of Ca in marine sediment and higher content of Ti in terrigenous sediment (e.g. Toucanne et *al.*, 2015). The aforementioned increase in grain size of core MOZ04-CSF19 is correlated with an increase in zirconium/rubidium (Zr/Rb) and Ca/Ti ratios, which suggest an enhancement in bottom current velocity and a weakening in the river input, respectively. Radiocarbon dating shows that the sandy layer is younger than 9 kyr BP (Figure 6B).

Channel

A longitudinal channel parallel to the bathymetric contours was identified in the middle of the contourite terrace (Figures 4 and 5). The channel is located at 155–170 m b.s.l., it is 134–580 m wide (mean width of 246 m) and incises the seafloor 2–13 m (mean channel incision depth of 9 m) (Figure 7). This channel was observed along 60 km of the Mozambican upper continental slope. It is limited at the south by a zone affected by a large submarine landslide (Figure 1B). North of the latitude 19°8′S, the channel seems to be more discontinuous, being replaced in some zones by dune fields, which will be described in the next section.

At large scale, the channel is considerably straight and parallel to the slope. However, its morphology often varies at small scale. The southern part of the channel is irregular and has a patchy distribution (Figure 7A). Its shallow flank is straighter than its deep flank (Figure 7A). North of 19°24′S, the channel

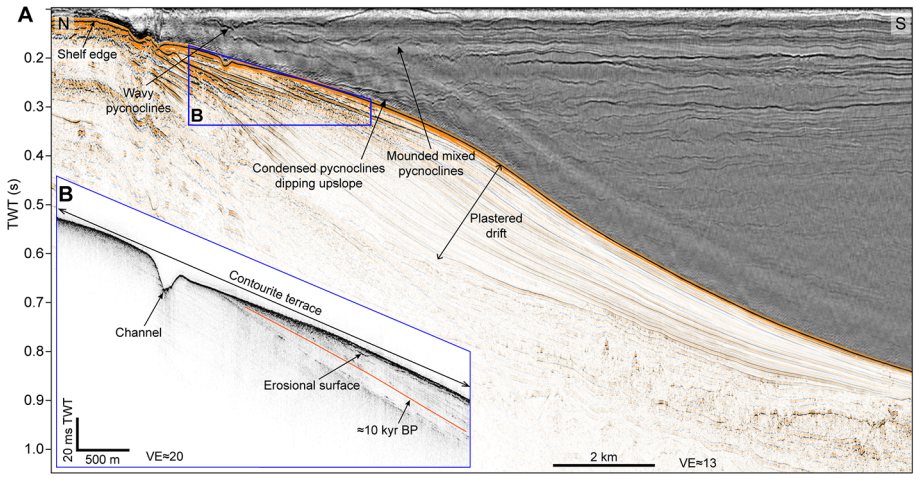

Figure 5. (A) Multi-channel high-resolution seismic reflection profile MOZ04-HR-108 of the water column (greyscale) and below the seafloor (colour scale), showing wavy reflections in the water column in the vicinity of the channel. See Figure 1B for profile location. (B) Sub-bottom profiler image MOZ04-SDS-108b, showing in detail the channel and the erosional truncations of the upper slope. [Colour figure can be viewed at wileyonlinelibrary.com]

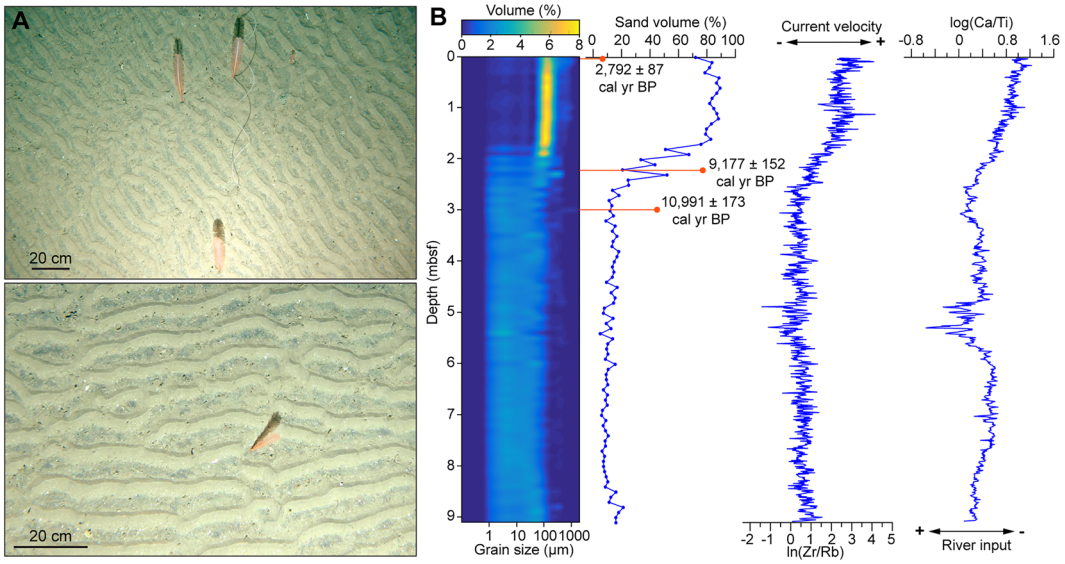

Figure 6. (A) Seafloor images at the core site characterized by straight- to sinuous-crested ripples. (B) Grain size distribution, sand volume, Napierian logarithm of the XRF zirconium/rubidium ratio and logarithm of the XRF calcium/titanium ratio of core MOZ04-CSF19. See Figures 1B and 2 for core location. [Colour figure can be viewed at wileyonlinelibrary.com]

becomes much straighter, showing continuous shallow and deep flanks and more regular channel widths and depths. A slightly mounded morphology is observed adjacent to the deep flank of the channel (Figure 7B).

Sand dunes

Dune fields are observed north of the channel between 120 and 250 m b.s.l. The real extension of the dune fields could not be determined due to the limited coverage of the multibeam bathymetry. The dune fields have not been directly sampled or observed with video. However, their depth and their location on a contourite terrace, on the top of a plastered drift, are similar to the environment where core MOZ04-CSF19 was collected, which is characterized by the presence of sandy deposits (Figures 4 and 6). Therefore, we consider that these dunes are probably mainly composed of sand.

Most of the dune crests are straight, although backscatter data show some barchanoid zones of high backscatter that could be interpreted as barchan dunes (Figure 8A). The dune crests are oriented oblique to the slope, with a main east–west (E–W) orientation and a superimposed secondary north–south (N–S) orientation (Figure 9). The deepest limit of the dune field is marked by an erosional surface at the seafloor, suggesting the presence of more energetic conditions in this area (Figure 8B). The dunes are medium to large (based on the classification of Ashley, 1990), with wavelengths between 20 and 150 m, heights between 0.15 and 1.50 m, and their size decreases upslope (Figures 8 and 10). The progressive change from erosional area to large dunes and finally to medium dunes suggests an upslope decrease of energy (Figure 8B). All the measured dunes are below the mean height-wavelength trend of Flemming (1988) (Figure 10). The asymmetry of the dunes suggests that they migrate obliquely upslope. Nevertheless, the secondary N–S orientation also suggests a secondary migration oblique to the slope, perpendicular to the main direction of

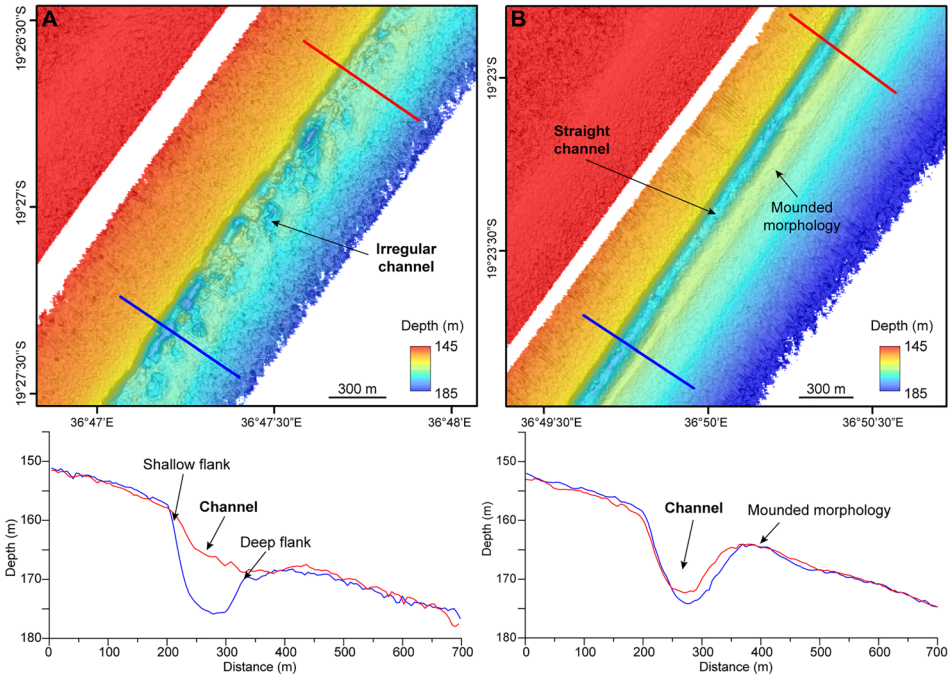

Figure 7. Multibeam bathymetry and bathymetric profiles of the channel characterized by an irregular shape in the southern part (A) and a straight shape in the northern part (B). See Figure 1B for location. [Colour figure can be viewed at wileyonlinelibrary.com]

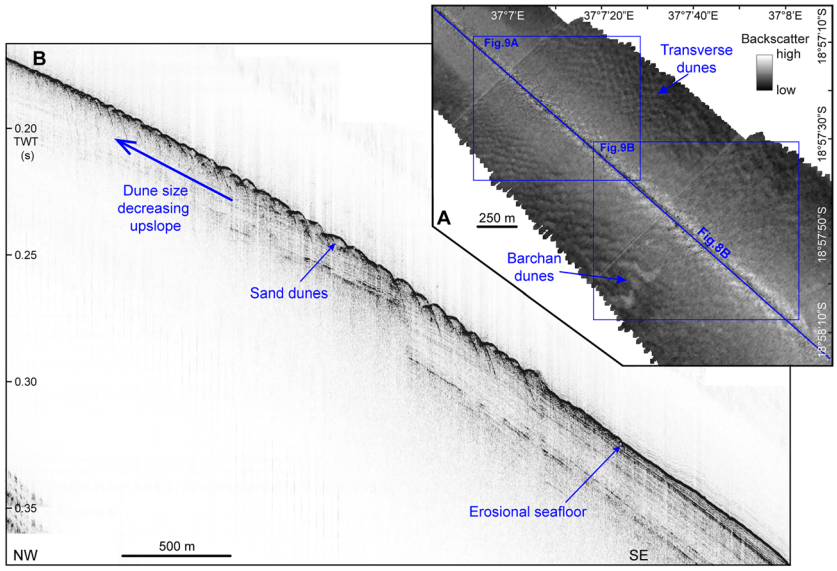

Figure 8. (A) Seafloor backscatter of the dune field. (B) Sub-bottom profiler image MOZ04-SBP-102a along the dune field, showing an erosional seafloor at the foot of the dune field and upslope migrating dunes. [Colour figure can be viewed at wileyonlinelibrary.com]

migration. The asymmetry of the secondary dunes is not as clear as for the main dunes, but they seem to migrate downslope (Figure 9A).

Evidences of internal waves from seismic data

Multi-channel high-resolution seismic reflection data show reflections within the water column that represent the oceanic stratification. The acoustic impedance is the relevant property for the reflection of acoustic waves, and it depends on sound speed and density (i.e. temperature and salinity) vertical variation in the water column. But it has been shown that the seismic reflectivity is mainly dominated by temperature variations in the water column (Sallarès et *al.*, 2009; Ker et *al.*, 2016). One temperature profile acquired at the same time as the seismic data in the Mozambique Channel shows a very good correlation between high amplitude reflections and peaks in temperature gradient between 0.15 and 0.20 s two-way travel time (TWT) (113–151 m b.s.l., using a sound velocity of 1512 m s^{-1} for time-depth conversion) (Figure 11). The zone at 0.20–0.25 s TWT (150–190 m b.s.l.) (characterized by chaotic and transparent reflections corresponds to low temperature gradient, i.e. a zone where the water column is well mixed (Figure 11)). A similar zone with chaotic reflections was observed above the contourite terrace of the upper slope at 0.15–0.30 s TWT (113–227 m b.s.l.) (Figure 5). This seismic profile shows a well-defined stratification of the water column characterized by relatively straight reflections in the offshore zone. In contrast, near the plastered drift, and especially above the

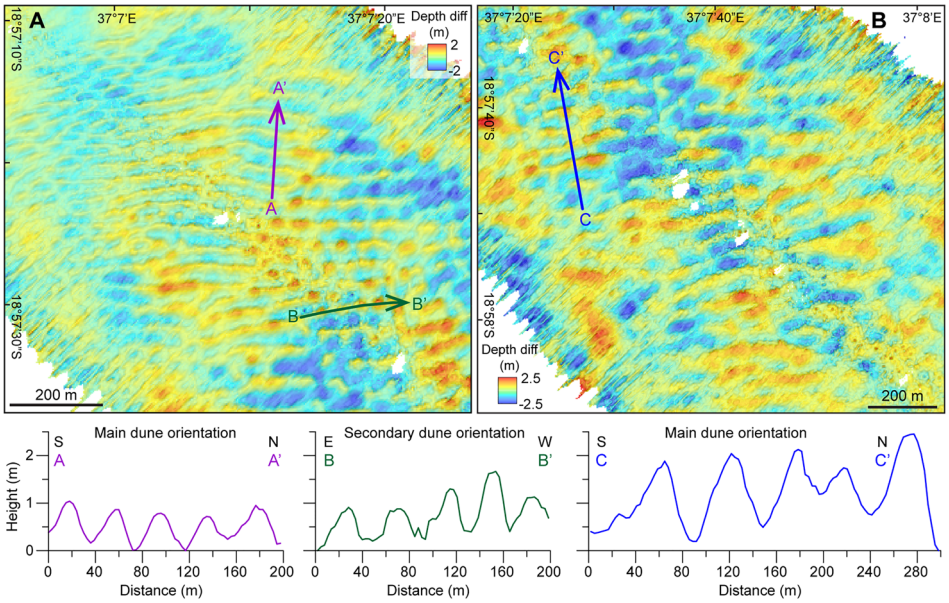

Figure 9. Differential bathymetry relative to the mean bathymetric surface of the upper part (A) and lower part (B) of the dune field, and bathymetric profiles of differential bathymetry to highlight dune morphologies. See Figure 8A for location. [Colour figure can be viewed at wileyonlinelibrary.com]

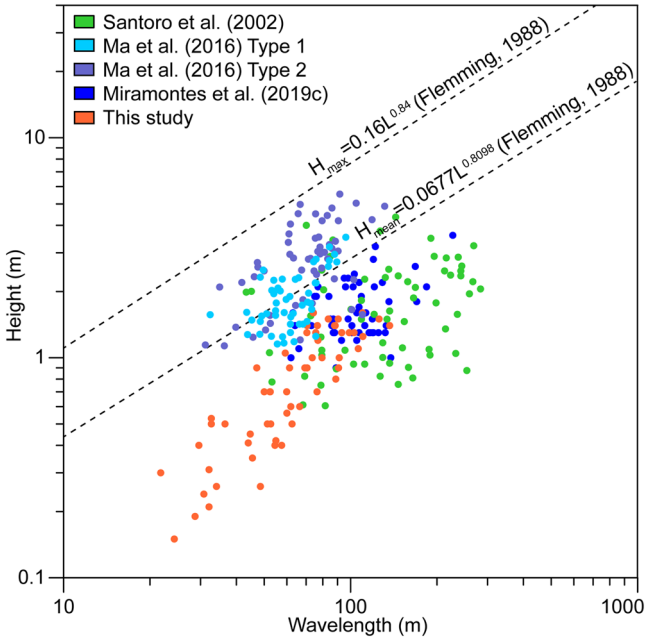

Figure 10. Height-wavelength diagram of the sand dunes measured in this study compared with sand dunes suggested to be influenced by internal solitary waves and internal tides in other settings (Santoro et *al.*, 2002; Ma et *al.*, 2016; Miramontes et *al.*, 2019c), and with the mean and maximum height–wavelength relationship after Flemming (1988). [Colour figure can be viewed at wileyonlinelibrary.com]

contourite terrace, the reflections become much more irregular and show a mounded shape. Wavy reflections, with almost the same extension as the channel, are also observed above this erosional feature (at about 0.15–0.20 s TWT, 113–151 m b.s.l.) (Figure 5).

The seismic profile acquired across the dune field shows more abundant small-scale undulations near the seafloor at the depth range of the dune field. Some of these undulations are grouped in packages that increase in amplitude onshore. This is characteristic of ISWs moving towards the slope (northwestwards in this case) (Figure 12B), which commonly have a first wave of high amplitude, followed by decreasing wave amplitude (Jackson et *al.*, 2012). Below this zone with ISWs, the reflections are inclined upwards in the vicinity of the eroded seafloor at about 0.3 s TWT (~227 m b.s.l.) (Figure 12A). Particular undulated high amplitude seismic reflections are also observed near the seafloor in the upper slope near the shelf edge at about 0.18 s TWT (~136 m b.s.l.) (Figure 11). These features could be interpreted as boluses generated by breaking internal waves (Bourgault et *al.*, 2014).

Slope criticality

The stratification of the water column above the upper slope was obtained from a XCTD profile, which shows a marked change in density at about 140 m w.d. that is linked to a change in temperature. The buoyancy frequency (N) increases from the surface reaching a maximum at 140 m b.s.l. and then it decreases with depth (Figure 13).

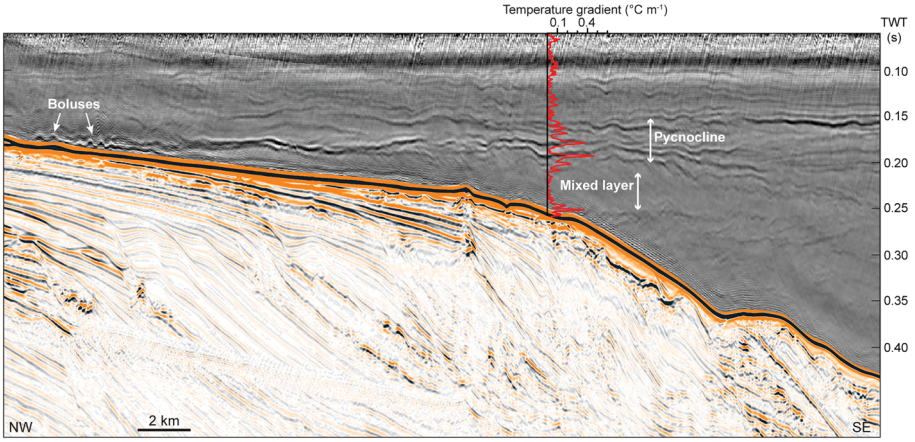

Figure 11. Multi-channel high-resolution seismic reflection profile MOZ04-HR-117 of the water column (greyscale) and the sub-seafloor (colour scale), and temperature gradient profile collected at the same time. Note the good correlation between high amplitude reflections in the water column and peaks in temperature gradient. [Colour figure can be viewed at wileyonlinelibrary.com]

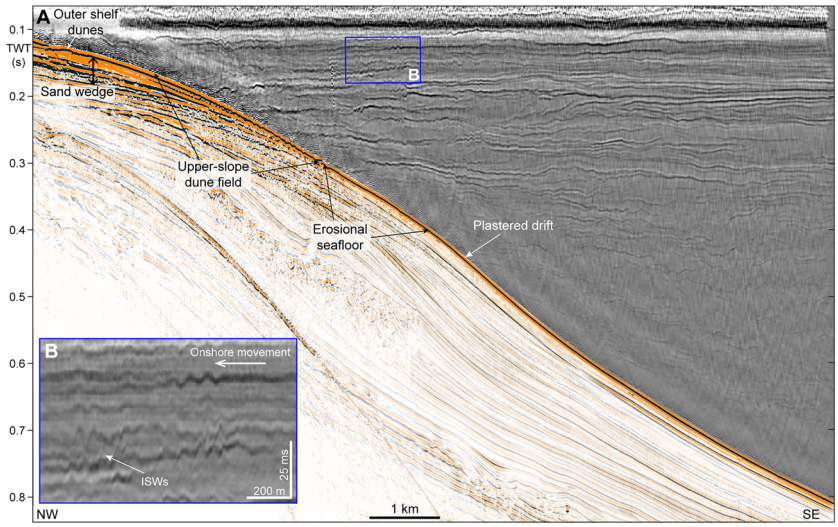

Figure 12. (A) Multi-channel high-resolution seismic reflection profile MOZ04-HR-102 of the water column (greyscale) and the sub-seafloor (colour scale), showing the dune field and internal solitary waves (ISWs) travelling onshore. (B) Detailed image of the ISWs. [Colour figure can be viewed at wileyonlinelibrary.com]

The ratio between slope angle (γ) and the characteristic angle for the semi-diurnal internal tides (c) was calculated for two different slope morphologies that characterize the upper continental slope of the Mozambican margin: (i) the convex shaped slope with a plastered drift, and a contourite terrace with a channel; and (ii) the less convex slope with a plastered drift and a dune field (Figure 14). Most of the upper slope is supercritical ($\gamma/c > 1$, reflective conditions) to semi-diurnal internal tides, the internal tide would thus be reflected downslope. However, some small zones in the slope, such as below the channel in the contourite terrace, as well as the zone of eroded slope below the dune field are under near-critical conditions (i.e. the slope angle is close to the natural internal wave propagation angle $\gamma/c \approx 1$, Figure 14). Under these conditions, energy is trapped at the seafloor and bottom velocities are intensified, often resulting in seafloor erosion and in the formation of nepheloid layers (Cacchione et *al.*, 2002).

Discussion

Within the contourite depositional system along the upper continental slope of the Mozambican margin, the plastered drift and the contourite terrace can be considered as first order (large-scale) sedimentary features, while channels and dunes can be defined as second order (small-scale) sedimentary features. Different oceanographic processes may be involved at distinct orders (scales) in generating sedimentary features, as proposed recently by Yin e*t al.* (2019), and they will be separately discussed in the following sections.

Oceanographic and sedimentary processes at the origin of large-scale features (plastered drifts and contourite terraces)

The main sediment source for the Mozambican slope is the Zambezi River. During sea-level low-stands, the Zambezi delta was located near the slope, and thus a large amount of fine-grained sediment was directly deposited on the slope (Figure 6; Schulz et *al.*, 2011). During sea-level high-stands the sediment is mainly transported northwards by alongshore currents, and then in part transported southwards along the upper continental slope by offshore currents (Figure 1C; Schulz et *al.*, 2011). As a consequence of a decrease in direct sediment supply and an increase in oceanic current intensity, a 2-m thick

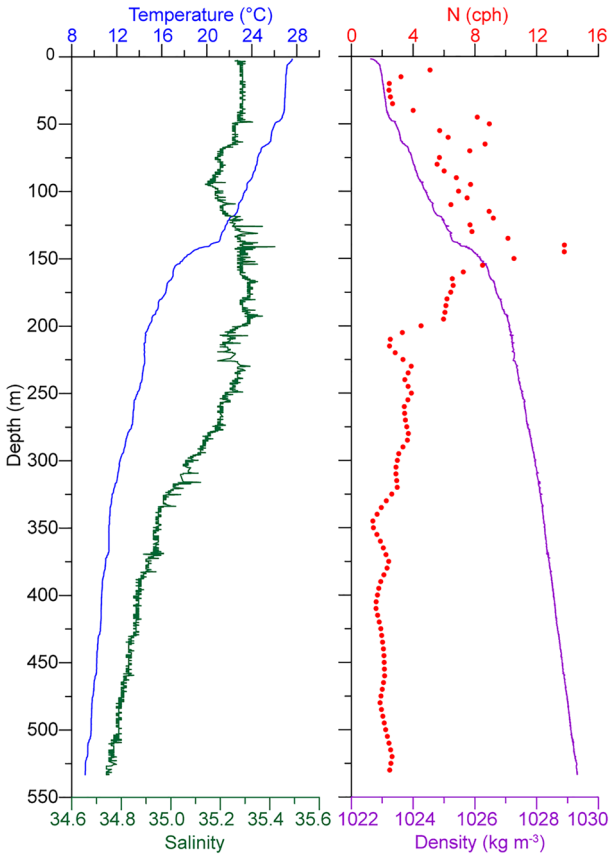

Figure 13. Profiles of temperature, salinity, density and buoyancy frequency (N). See Figure 1B for location. [Colour figure can be viewed at wileyonlinelibrary.com]

winnowed sandy layer formed on the contourite terrace of the upper slope (Figure 6).

Modelling results show that on average geostrophic currents flow southwest along the upper Mozambican continental margin (Flemming and Kudrass, 2018; Miramontes et *al.*, 2019a). Bottom shear stresses related to geostrophic currents are higher on the continental shelf and upper slope, and then they generally decrease with depth (Figures 15A and 15B). The contourite terrace may thus be under the influence of intense geostrophic currents on the upper slope, and the plastered drift would develop in the adjacent area basinwards, where weaker geostrophic currents allow sediment deposition (Figures 4 and 5). Similar distribution of bottom currents and sedimentary features have already been observed in the western Mediterranean Sea, where contourite terraces are usually in a zone affected by intense bottom currents, whereas the adjacent plastered drifts are in a zone of weak bottom currents (Cattaneo et *al.*, 2017; Miramontes et *al.*, 2019b).

Oceanographic processes at the origin of small-scale features (channel and dunes)

The channel and the dunes observed in the upper slope of the Mozambique Channel are located in a similar water depth as the pycnocline: the channel is at 155–170 m b.s.l. (Figure 7), the dunes at 120–250 m b.s.l. (Figure 8) and the pycnocline at 100–200 m b.s.l., with the strongest change in density at about 140 m b.s.l. (Figure 13). This co-existence may suggest a relationship between the formation of these sedimentary features and oceanographic processes related to the pycnocline dynamics, especially internal waves. Here, we discuss possible mechanisms that may have originated these sedimentary features.

Manders e*t al.* (2004) observed internal tides in the Mozambique Channel that were formed on continental slope of Mozambique. Internal tidal beams generated east of the study area, could be directed to the Mozambican slope. The bottom criticality analysis performed on this area shows that most of the slope is under reflective conditions. The tidal beams would thus be reflected downslope. Therefore, this process could not explain the formation of the upslope migrating dunes, although it could have an effect in remobilizing sediment in the upper slope and in generating the secondary dunes (Figure 9). The zone below the channel is under near-critical conditions. The reflection of internal tides at a slope with critical angle can cause significant turbulence at the seafloor and lead to enhanced bottom current velocities (Cacchione et *al.*, 2002; Zhang et *al.*, 2008; Gayen and Sarkar, 2010). This could explain the observed broad erosion in the contourite terrace below the channel, but not focused erosion within the channel (Figure 5).

Da Silva e*t al.* (2009) observed ISWs being formed in the southern part of the Sofala Bank continental slope and further offshore by interaction of the reflected internal tidal beam with the thermocline, but they did not identify any ISWs from Envisat advanced synthetic aperture radar (ASAR) imagery in our study area (Figure 1A). In the area where ISWs were identified, the pycnocline was located at 60 m b.s.l. (da Silva et *al.*, 2009). In contrast, in our study area, the pycnocline is deeper, at about 140 m b.s.l. (Figure 13). ISWs propagating in this deeper pycnocline may not significantly disturb the sea surface, and may thus not be visible from satellite imagery.

Seismic profiles show evidences of ISWs propagating in the pycnocline near the zones with the channel and the dunes with a landward direction (Figures 5 and 12). Such ISWs could

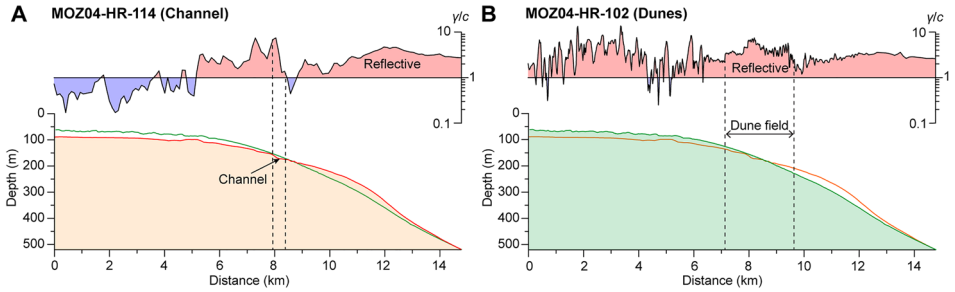

Figure 14. Ratio between seafloor slope angle (γ) and characteristic angle for semi-diurnal internal tides (c), and bathymetric profiles of two different slope profiles: (A) as seismic profile MOZ04-HR-114 characterized by a channel (orange profile); (B) as seismic profile MOZ04-HR-102 characterized by a dune field (green profile). The bathymetric profile corresponding to each γ/c graph is filled with colour and the other bathymetric profile is also plotted for comparison. [Colour figure can be viewed at wileyonlinelibrary.com]

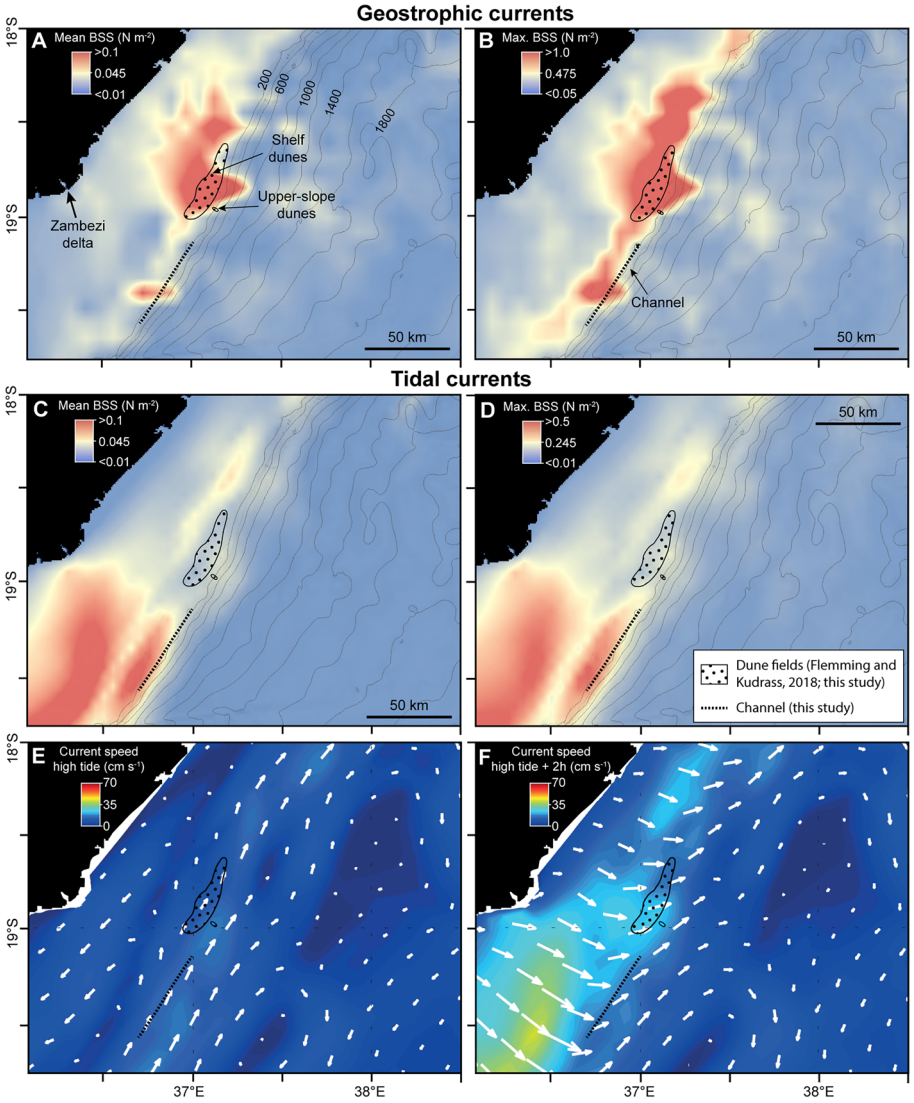

Figure 15. (A) Mean and (B) maximum bottom shear stress (BSS) related to geostrophic currents from the ROMS model (modified after Miramontes et *al.*, 2019a; Thiéblemont et *al.*, 2019). (C) Mean and (D) maximum BSS related to tidal currents simulated with the ROMS model (modified after Chevane et *al.*, 2016). Depth contours are shown every 200 m. Vertically average barotropic tidal currents during (E) high tide and (F) two hours after high tide (modified after Chevane et *al.*, 2016). The area filled with black dots represents the dune fields mapped by Flemming and Kudrass (2018) and by the present study. The dashed black line represents the channel identified in the present study. [Colour figure can be viewed at wileyonlinelibrary.com]

have been originated by the impinging on the pycnocline of internal tide beams that move landward. The partial trapping of these internal tide energy within the pycnocline could generate ISWs as the ones observed in the seismic profiles (Mercier et al., 2012).

Seismic data of the water column also revealed the formation of boluses migrating onshore right below the shelf edge at about 140 m b.s.l. (Figure 11). Boluses are often formed by shoaling ISWs. They are powerful processes that can resuspend sediment and generate nepheloid layers (Bourgault et *al.*, 2014). Shoaling and breaking ISWs slope may contribute to the broad erosion in the contourite terraces (Figures 4 and 5). However, this process cannot explain focused erosion within the channel (Figures 5 and 7). The formation of the channel may be related to landward propagating ISWs arrested by barotropic tidal currents. The channel is located in an area with strong barotropic tidal currents (Figures 15C and 15D). During ebb tide, barotropic tidal currents are directed towards the southeast, almost perpendicular to the slope and to the channel (Figure 15F). If the barotropic tidal current (flowing basinwards) is equal or greater than the propagation velocity of an ISW travelling in the pycnocline landwards, the ISWs would be arrested, resulting in increased amplitude and increased current velocity near the seafloor, and internal hydraulic jumps may occur (Figure 16A; Farmer and Smith, 1980; Farmer and Armi, 1999; Bruno et *al.*, 2002). The bottom current induced by the arrested ISW would affect a small area across-slope that would not be larger than the wavelength of the ISW. Since the stratification of the water column does not show important seasonal changes in the Mozambique Channel (da Silva et *al.*, 2009), this localized area may continuously be eroded by arrested internal waves, especially during spring tides, when the barotropic tidal currents are stronger (Farmer and Smith, 1980; Vázquez et al., 2008). The erosion will thus only affect a small area of the slope, which will be always the same if the general slope geometry does not change, resulting in a continuous and linear contourite channel (Figures 4 and 7).

In contrast to the zone with the channel, barotropic tidal currents are weak in the zone with the dune field (Figures 15C and 15D), suggesting that ISWs may not be arrested by barotropic flow in this area. The velocity direction of ISWs of depressions in their lower part is the opposite to the direction of propagation of ISWs. When the thickness of the upper layer of the pycnocline ($h1$) is greater than the thickness of the lower layer

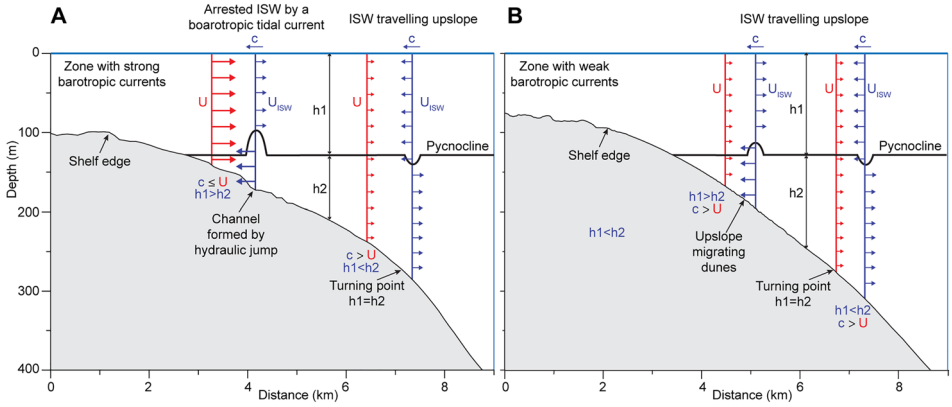

Figure 16. Schematic model of the processes that may be at the origin of the observed sedimentary features: (A) the channel may be formed by a hydraulic jump generated by arrested internal solitary waves (ISWs), when the barotropic tidal current (U) is equal or greater than the propagation velocity of the ISW (c); (B) the upslope migrating dunes may be formed by upslope bottom currents induced by ISWs of elevation. Here, $h1$ and $h2$ are the thickness of the layers above and below the pycnocline. The red arrows represent the barotropic current (U) and the blue arrows represent the currents induced by the ISW (U_{ISW}). [Colour figure can be viewed at wileyonlinelibrary.com]

($h2$), the polarity of the ISWs changes, becoming an ISWs of elevation (Figure 16B). The horizontal zone where this change of polarity occurs is called a turning or critical point (Lamb, 2014). The current velocity direction in the lower part of ISWs of elevation is the same as the direction of propagation of the ISW. In the case of ISWs travelling landwards, the currents near the seafloor would be in the upslope direction. The propagation of ISWs of elevation in the pycnocline may be at the origin of the upslope migrating dunes observed in the upper slope (Figures 8 and 16B).

The secondary dunes perpendicular to the upslope migrating dunes may have a different origin. They may be formed by the ebb current, which has a southeast-east direction in the area of the dunes (Figure 15F). They could be also related to the eddies that commonly affect the Mozambican slope (Halo et *al.*, 2014) or by the reflection of internal tides under reflective conditions, as suggested for instance for downslope migrating dunes in the South China Sea (Ma et *al.*, 2016). Although the dominant component of sediment transport is upslope (probably induced by ISWs), resulting in the formation of upslope migrating dunes, part of the sediment may be transported back downslope by other processes, generating the perpendicular secondary dunes. The fact that processes with different directions of sediment transport affect the same area could explain the low height–wavelength ratio of the main dunes, which lies below the global mean height–wavelength ratio compiled by Flemming (1988) (Figure 10). The smaller dunes show a bigger difference in height compared to the mean trend than the bigger dunes; i.e. the height of the dunes with wavelengths of 30 to 50 m is 61–65% lower than the height of the mean trend, while the height of the dunes with wavelengths of 90 to 100 m is 54–55% lower than the height of the mean trend (Figure 10). This could be due to the fact that the smaller dunes are shallower and thus more affected by the downslope flow, which may be stronger in the shallowest part of the slope (for instance barotropic tidal current intensity decreases with depth (Figures 15C and 15D). On the contrary, the deeper dunes may be in an area where the upslope flow is stronger, inducing the generation of larger dunes; and the downslope flow weaker, eroding less the crests of the dunes. The dunes suggested to be formed by internal waves in other studies (Santoro et *al.*, 2002; Droghei et *al.*, 2016; Ma et *al.*, 2016; Miramontes et *al.*, 2019c) often lie below the mean height–wavelength trend (Figure 10). This indicates that these dunes may form in settings where the direction of the bottom current changes, first generating the dune and then eroding its crest and moving the sediment to the trough, reducing dune height without affecting dune length.

Cyclicity in small-scale sedimentary features formation

The channel observed on the present seafloor of the Mozambican slope is younger than 9 kyr BP, based on correlation with core MOZ04-CSF19 (Figure 6B). The absence of sediment drape in the channel, suggests that its formation is active at present (Figures 4 and 5). Another ancient channel could be identified in the subsurface in the seismic data (Figure 4). The ancient channel is younger than the bottom of Site U1477 from IODP expedition 361, that was dated with a maximum age of ~200 ka (Hall et *al.*, 2016). We thus suggest that the ancient channel was probably formed during the previous sea-level high-stand (MIS5). During sea-level low-stands the Zambezi River discharges large amounts of fine-grained material that accumulate on shelf edge and continental slope (Figure 6; Schulz et *al.*, 2011). Even if internal waves were probably also affecting the upper slope during sea-level low-stands, high sedimentation rates from the delta might overcome the erosion and transport capacity of internal waves and therefore no contourite channel could develop. The presence of this ancient channel proves that internal waves may have cyclic imprints on continental slopes, as suggested for instance in the formation of sediment waves along the Israeli continental slope (Reiche et *al.*, 2018).

Conclusions

The contourite depositional system of the Mozambican upper slope is mainly composed of large-scale sedimentary features (a plastered drift and a contourite terrace), superimposed by small-scale sedimentary features (a channel and sand dunes) revealed by high resolution multibeam bathymetry and seismic data. Although this classification and superposition of sedimentary features at different scales may apply to any contourite depositional system in the world, they are not often observed due to the lack of high-resolution data. The detailed observations of the seafloor and the water column shown in this study provide insights into the type of sedimentary features that can be found on upper continental slopes and into the oceanographic processes at their origin.

In this study we show that in the upper slope of the Mozambican margin, large-scale sedimentary features (plastered drifts and contourite terraces) are probably generated by geostrophic currents, whereas small-scale sedimentary features (channels and sand dunes) may be formed by internal waves. Internal solitary waves arrested by barotropic tidal currents, may generate a hydraulic jump and induce increased erosion in a localized zone of the upper continental slope, generating the channel that was observed along 60 km at 155–170 m b.s.l. In the zones where barotropic tidal currents are weak, internal solitary waves are not arrested. Internal solitary waves of elevation can thus propagate shelfwards, generating upslope-flowing bottom currents, which may be at the origin of the field of medium to large dunes observed at 120–250 m b.s.l. The main dune crests migrate obliquely upslope and decrease in size in the same direction. Secondary dunes are superimposed to the main dunes, with crest oriented perpendicularly to the main crests. These dunes may be formed by other oceanographic processes, such as downslope reflection of internal tides under reflective conditions, barotropic tidal currents or eddies. These processes may also erode the main dune crests, reducing their height without affecting their wavelength.

This study evidences the impact of internal waves on the sedimentation and morphology of upper continental margins by combining geophysical and sedimentological data, and numerical modelling. *In situ* measurements and high-resolution modelling of oceanographic processes and sediment resuspension are necessary to further understand and quantify the impact of internal waves in sediment transport on continental slopes.

Acknowledgements—The authors thank the Captain, crew and onboard scientific team of the PAMELA-MOZ04 survey onboard the R/V *Pourquoi pas?*. D. Belleney, B. Dennielou, A. Roubi and M. Rovere (IFREMER) are warmly thanked for core processing. The oceanographic survey PAMELA-MOZ04 and Elda Miramontes' Post-Doctoral fellowship were co-funded by TOTAL and IFREMER as part of the PAMELA (PAssive Margin Exploration Laboratories) scientific project. The PAMELA project is a scientific project led by Ifremer and TOTAL in collaboration with Université de Bretagne Occidentale, Université Rennes 1, Université Pierre and Marie Curie, CNRS and IFPEN. The authos acknowledge the use of imagery from the NASA Worldview application (https://worldview.earthdata.nasa.gov), part of the NASA Earth Observing System Data and Information System (EOSDIS). The PhD thesis of A. Thiéblemont was funded by TOTAL as part of the Frontier Exploration research programme. The research of F. J. Hernández-Molina was conducted in the framework of 'The Drifters Research Group' of the Royal Holloway University of London (UK) and it is related to the projects CTM 2012-39599-C03, CGL2016-80445-R, and CTM2016-75129-C3-1-R. The authors thank the guest editor C. Winter and two anonymous reviewers for their valuable suggestions that improved this manuscript.

Conflict of Interest Statement

The authors declare that they have no conflict of interest.

Data Availability Statement

Research data are not shared.

References

Ashley GM. 1990. Classification of large-scale subaqueous bedforms: a new look at an old problem. *Journal of Sedimentary Petrology* **60**: 160–172.

Bahr A, Jiménez-Espejo FJ, Kolasinac N, Grunert P, Hernández-Molina FJ, Röhl U, Voelker AHL, Escutia C, Stow DAV, Hodell D, Alvarez-Zarikian CA. 2014. Deciphering bottom current velocity and paleoclimate signals from contourite deposits in the Gulf of Cádiz during the last 140 kyr: an inorganic geochemical approach. *Geochemistry, Geophysics, Geosystems* **15**: 3145–3160.

Baines PG. 1982. On internal tide generation models. *Deep Sea Research Part A. Oceanographic Research Papers* **29**: 307–338.

Beiersdorf H, Kudrass HR, von Stackelberg U. 1980. Placer deposits of ilmenite and zircon on the Zambezi Shelf. *Geologisches Jahrbuch Reihe D* **36**: 1–85.

Bourgault D, Morsilli M, Richards C, Neumeier U, Kelley DE. 2014. Sediment resuspension and nepheloid layers induced by long internal solitary waves shoaling orthogonally on uniform slopes. *Continental Shelf Research* **72**: 21–33.

Breitzke M, Wiles E, Krocker R, Watkeys MK, Jokat W. 2017. Seafloor morphology in the Mozambique Channel: evidence for long-term persistent bottom-current flow and deep-reaching eddy activity. *Marine Geophysical Research* **38**: 241–269.

Bruno M, Alonso JJ, Cózar A, Vidal J, Ruiz-Cañavate A, Echevarría J, Ruiz J. 2002. The boiling-water phenomena at Camarinal Sill, the Strait of Gibraltar. *Deep-Sea Research Part II* **49**: 4097–4113.

Cacchione DA, Drake DE. 1986. Nepheloid layers and internal waves over continental shelves and slopes. *Geo-Marine Letters* **6**: 147–152.

Cacchione DA, Pratson LF, Ogston AS. 2002. The shaping of continental slopes by internal tides. *Science* **269**: 724–727.

Cattaneo A, Miramontes E, Samalens K, Garreau P, Caillaud M, Marsset B, Corradi N, Migeon S. 2017. Contourite identification along Italian margins: the case of the Portofino drift (Ligurian Sea). *Marine and Petroleum Geology* **87**: 137–147.

Chevane CM, Penven P, Nehama FPJ, Reason CJC. 2016. Modelling the tides and their impacts on the vertical stratification over the Sofala Bank, Mozambique. *African Journal of Marine Science* **38**: 465–479.

DiMarco SF, Chapman P, Nowlin WD, Jr, Hacker P, Donohue K, Luther M, Johnson GC, Toole J. 2002. Volume transport and property distributions of the Mozambique Channel. *Deep Sea Research Part II: Topical Studies in Oceanography* **49**: 1481–1511.

Droghei R, Falcini F, Casalbore D, Martorelli E, Mosetti R, Sannino G, Santoreli R, Chiocci FL. 2016. The role of internal solitary waves on deep-water sedimentary processes: the case of up-slope migrating sediment waves off the Messina Strait. *Scientific Reports* **6**: 36376. https://doi.org/10.1038/srep36376.

Farmer D, Armi L. 1999. The generation and trapping of solitary waves over topography. *Science* **283**: 188–190.

Farmer DM, Smith JD. 1980. Tidal interaction of stratified flow with a sill in Knight Inlet. *Deep-Sea Research* **27A**: 239–245.

Faugères J-C, Stow DAV. 2008. Contourite drifts: nature, evolution and controls. In *Contourites*, Rebesco M, Camerlenghi A (eds), Developments in Sedimentology 60. Elsevier: Amsterdam; 257–288.

Fekete BM, Vörösmarty CJ, Grabs W. 1999. *Global Composite Runoff Fields Based on Observed River Discharge and Simulated Water Balances*, WMO – Global Runoff Data Centre Report, 22. Global Runoff Data Centre: Koblenz.

Fierens R, Droz L, Toucanne S, Raisson F, Jouet G, Babonneau N, Miramontes E, Landurain S, Jorry S. 2019. Late Quaternary geomorphology and sedimentary processes in the Zambezi turbidite system (Mozambique Channel). *Geomorphology* **334**: 1–28.

Flemming BW. 1988. Zur Klassifikation subaquatischer, strömungstransversaler Transportkörper. *Bochumer Geologische und Geotechnische Arbeit* **29**: 93–97.

Flemming BW, Kudrass HR. 2018. Large dunes on the outer shelf off the Zambezi Delta, Mozambique: evidence for the existence of a Mozambique Current. *Geo-Marine Letters* **38**: 95–106.

Gayen B, Sarkar S. 2010. Turbulence during the generation of internal tide on a critical slope. *Physical Review Letters* **104**: 218502. https://doi.org/10.1103/PhysRevLett.104.218502.

Gordon AL. 1986. Inter-ocean exchange of thermocline water. *Geophysical Research Letters* **91**: 5037–5046.

Hall IR, Hemming SR, LeVay LJ, the Expedition 361 Scientists. 2016. Expedition 361 Preliminary Report: South African Climates (Agulhas LGM Density Profile). International Ocean Discovery Program. https://doi.org/10.14379/iodp.pr.361.2016.

Halo I, Backeberg B, Penven P, Ansorge I, Reason C, Ullgren JE. 2014. Eddy properties in the Mozambique Channel: a comparison between observations and two numerical ocean circulation models. *Deep Sea Research Part II: Topical Studies in Oceanography* **100**: 38–53.

Hernández-Molina FJ, Llave E, Stow DAV. 2008. Continental slope contourites. In *Contourites*, Rebesco M, Camerlenghi A (eds), Developments in Sedimentology 60. Elsevier: Amsterdam; 379–408.

Hernández-Molina FJ, Paterlini M, Violante R, Marshall P, de Isasi M, Somoza L, Rebesco M. 2009. Contourite depositional system on the Argentine Slope: an exceptional record of the influence of Antarctic water masses. *Geology* **37**(6): 507–510.

Hernández-Molina FJ, Wåhlin A, Bruno M, Ercilla G, Llave E, Serra N, Roson G, Puig P, Rebesco M, Van Rooij D, Roque C, González-Pola C, Sánchez F, Gómez M, Preu B, Schwenk T, Hanebuth TJJ, Sánchez-Leal RF, García Lafuente J, Brackenridge RE, Juan C, Stow DAV, Sánchez-González JM. 2016a. Oceanographic processes and products around the Iberian margin: a new multidisciplinary approach. *Marine Geology* **378**: 127–156.

Hernández-Molina FJ, Soto M, Piola AR, Tomasini J, Preu B, Thompson P, Badalini G, Creaser A, Violante RA, Morales E, Paterlini M, De Santa Ana H. 2016b. A contourite depositional system along the Uruguayan continental margin: sedimentary, oceanographic and paleoceanographic implications. *Marine Geology* **378**: 333–349.

Hernández-Molina FJ, Campbell S, Badalini G, Thompson P, Walker R, Soto M, Conti B, Preu B, Thieblemont A, Hyslop L, Miramontes E, Morales E. 2017. Large bedforms on contourite terraces: sedimentary and conceptual implications. *Geology* **46**: 27–30.

Hunter S, Wilkinson D, Louarn E, McCave IN, Rohling E, Stow DA, Bacon S. 2007. Deep western boundary current dynamics and associated sedimentation on the Eirik Drift, Southern Greenland Margin. *Deep Sea Research Part I: Oceanographic Research Papers* **54**: 2036–2066.

Jackson CR, da Silva JCB, Jeans G. 2012. The generation of nonlinear internal waves. *Oceanography* **25**: 108–123.

Jouet G, Deville E. 2015. PAMELA-MOZ04 cruise, RV Pourquoi pas? https://doi.org/10.17600/15000700.

Ker S, Le Gonidec Y, Marie L. 2016. Multifrequency seismic detectability of seasonal thermoclines assessed from ARGO data. *Journal of Geophysical Research: Oceans* **121**: 6035–6060.

Kolla V, Eittreim S, Sullivan L, Kostecki JA, Burckle LH. 1980. Current-controlled, abyssal microtopography and sedimentation in Mozambique Basin, southwest Indian Ocean. *Marine Geology* **34**: 171–206.

Lamb KG. 2014. Internal wave breaking and dissipation mechanisms on the Continental Slope/Shelf. *Annual Review of Fluid Mechanics* **46**: 231–254.

de Lavergne C, Madec G, Capet X, Guillaume Maze G, Roquet F. 2016. Getting to the bottom of the ocean. *Nature Geoscience* **9**: 857–858.

van der Lubbe JJL, Tjallingii R, Prins MA, Brummer GJA, Jung SJA, Kroon D, Schneider RR. 2014. Sedimentation patterns off the Zambezi River over the last 20,000 years. *Marine Geology* **355**: 189–201.

Lutjeharms JRE. 2006. *The Agulhas Current, Volume 1*. Springer-Verlag: Berlin.

Lutjeharms JRE, Biastoch A, van der Werf PM, Ridderinkhof H, de Ruijter WPM. 2012. On the discontinuous nature of the Mozambique current. *South African Journal of Science* **108**: 01–05.

Ma X, Yan J, Hou Y, Lin F, Zheng X. 2016. Footprints of obliquely incident internal solitary waves and internal tides near the shelf break in the northern South China Sea. *Journal of Geophysical Research: Oceans* **121**: 8706–8719.

Magalhaes JM, da Silva JCB, New AL. 2014. Internal solitary waves system in the Mozambique Channel. In *Remote Sensing of the African Seas*, Barale V, Gade M (eds). Springer: Dordrecht; 263–284.

Manders AMM, Maas LRM, Gerkema T. 2004. Observations of internal tides in the Mozambique Channel. *Journal of Geophysical Research* **109**: C12034. https://doi.org/10.1029/2003JC002187.

Mercier MJ, Mathur M, Gostiaux L, Gerkema T, Magalhães JM, Da Silva JCB, Dauxois T. 2012. Soliton generation by internal tidal beams impinging on a pycnocline: laboratory experiments. *Journal of Fluid Mechanics* **704**: 37–60. https://doi.org/10.1017/jfm.2012.191.

Miramontes E, Penven P, Fierens R, Droz L, Toucanne S, Jorry SJ, Jouet G, Pastor L, Silva Jacinto R, Gaillot A, Giraudeau J, Raisson F. 2019a. The influence of bottom currents on the Zambezi Valley morphology (Mozambique Channel, SW Indian Ocean): in situ current observations and hydrodynamic modelling. *Marine Geology* **410**: 42–55.

Miramontes E, Garreau P, Caillaud M, Jouet G, Pellen R, Hernández-Molina FJ, Clare MA, Cattaneo A. 2019b. Contourite distribution and bottom currents in the NW Mediterranean Sea: coupling seafloor geomorphology and hydrodynamic modelling. *Geomorphology* **333**: 43–60.

Miramontes E, Jorry SJ, Jouet G, Counts JW, Courgeon S, Le Roy P, Guerin C, Hernández-Molina FJ. 2019c. Deep marine dunes on drowned isolated carbonate terraces (Mozambique Channel, SW Indian Ocean). *Sedimentology* **66**: 1222–1242.

Preu B, Hernández-Molina FJ, Violante R, Piola AR, Paterlini CM, Schwenk T, Voigt I, Krastel S, Spiess V. 2013. Morphosedimentary and hydrographic features of the northern Argentine margin: the interplay between erosive, depositional and gravitational processes and its conceptual implications. *Deep Sea Research Part I: Oceanographic Research Papers* **75**: 157–174.

Puig P, Palanques A, Guillén J, El Khatab M. 2004. Role of internal waves in the generation of nepheloid layers on the northwestern Alboran slope: implications for continental margin shaping. *Journal of Geophysical Research: Oceans* **109**(C9): C09011. https://doi.org/10.1029/2004JC002394.

Quartly GD, de Cuevas BA, Coward AC. 2013. Mozambique Channel eddies in GCMs: a question of resolution and slippage. *Ocean Modelling* **63**: 56–67.

Rebesco M, Hernández-Molina FJ, Van Rooij D, Wåhlin A. 2014. Contourites and associated sediments controlled by deep-water circulation processes: state-of-the-art and future considerations. *Marine Geology* **352**: 111–154.

Reiche S, Hübscher C, Brenner S, Betzler C, Hall JK. 2018. The role of internal waves in the late Quaternary evolution of the Israeli continental slope. *Marine Geology* **406**: 177–192.

Reimer PJ, Bard E, Bayliss A, Beck JW, Blackwell PG, Ramsey CB, Buck CE, Cheng H, Edwards RL, Friedrich M, Grootes PM, Guilderson TP, Haflidason H, Hajdas I, Hatte C, Heaton TJ, Hoffmann DL, Hogg AG, Hughen KA, Kaiser KF, Kromer B, Manning SW, Niu M, Reimer RW, Richards DA, Scott EM, Southon JR, Staff RA, Turney CSM, van der Plicht J. 2013. IntCal13 and Marine13 radiocarbon age calibration curves 0–50,000 years cal BP. *Radiocarbon* **55**: 1869–1887.

Ribó M, Puig P, Muñoz A, Lo Iacono C, Masqué P, Palanques A, Acosta J, Guillén J, Gómez Ballesteros M. 2016. Morphobathymetric analysis of the large fine-grained sediment waves over the Gulf of Valencia continental slope (NW Mediterranean). *Geomorphology* **253**: 22–37.

de Ruijter WPM, Ridderinkhof H, Lutjeharms JRE, Schouten MW, Veth C. 2002. Observations of the flow in the Mozambique Channel. *Geophysical Research Letters* **29**(10): 1502. https://doi.org/10.1029/2001GL013714.

Sallarès V, Biescas B, Buffett G, Carbonell R, Dañobeitia JJ, Pelegrí JL. 2009. Relative contribution of temperature and salinity to ocean acoustic reflectivity. *Geophysical Research Letters* **36**: L00D06. https://doi.org/10.1029/2009GL040187.

Santoro VC, Amore E, Cavallaro L, Cozzo G, Foti E. 2002. Sand waves in the Messina Strait, Italy. *Journal of Coastal Research* **36**: 640–653.

Schlitzer R. 2018. Ocean Data View, odv.awi.de.

Schulz H, Lückge A, Emeis K, Mackensen A. 2011. Variability of Holocene to Late Pleistocene 656 Zambezi riverine sedimentation at the upper continental slope off Mozambique, 15°–21°S. *Marine Geology* **286**: 21–34.

da Silva JCB, New AL, Magalhaes JM. 2009. Internal solitary waves in the Mozambique Channel: observations and interpretation. *Journal of Geophysical Research: Oceans* **114**: C05001. https://doi.org/10.1029/2008JC005125.

Ternon JF, Roberts MJ, Morris T, Hancke L, Backeberg B. 2014. In situ measured current structures of the eddy field in the Mozambique Channel. *Deep Sea Research Part II: Topical Studies in Oceanography* **100**: 10–26.

Thiéblemont A, Hernández-Molina FJ, Miramontes E, Raisson F, Penven P. 2019. Contourite depositional systems along the Mozambique Channel: the interplay between bottom currents and sedimentary processes. *Deep-Sea Research Part I: Oceanographic Research Papers* **147**: 79–99.

Toucanne S, Minto'o CMA, Fontanier C, Bassetti MA, Jorry SJ, Jouet G. 2015. Tracking rainfall in the northern Mediterranean borderlands during sapropel deposition. *Quaternary Science Reviews* **129**: 178–195.

Ullgren JE, van Aken HM, Ridderinkhof H, de Ruijter WPM. 2012. The hydrography of the Mozambique Channel from six years of continuous temperature, salinity, and velocity observations. *Deep Sea Research Part I: Oceanographic Research Papers* **69**: 36–50.

Vázquez A, Bruno M, Izquierdo A, Macías D, Ruiz-Cañavate A. 2008. Meteorologically forced subinertial flows and internal wave generation at the main Sill of the Strait of Gibraltar. *Deep-Sea Research Part I* **55**: 1277–1283.

Walford H, White N, Sydow J. 2005. Solid sediment load history of the Zambezi Delta. *Earth and Planetary Science Letters* **238**: 49–63.

Weijer W, de Ruijter WPM, Dijkstra HA, van Leeuwen PJ. 1999. Impact of interbasin exchange on the Atlantic overturning circulation. *Journal of Physical Oceanography* **29**: 2266–2284.

Wiles E, Green AN, Watkeys MK, Jokat W. 2017. Zambezi continental margin: compartmentalized sediment transfer routes to the abyssal Mozambique Channel. *Marine Geophysical Research* **38**: 227–240.

Wyrtki K. 1973. Physical oceanography in the Indian Ocean. In *Ecological Studies. Analysis and Synthesis*, Zeitzschel B (ed). Springer-Verlag: Berlin; 18–36.

Yin S, Hernández-Molina FJ, Zhang W, Li J, Wang L, Ding W, Ding W. 2019. The influence of oceanographic processes on contourite features: a multidisciplinary study of the northern South China Sea. *Marine Geology* **415**: 105967. https://doi.org/10.1016/j.margeo.2019.105967.

You Y. 1997. Seasonal variations of thermocline circulation and ventilation in the Indian Ocean. *Journal of Geophysical Research* **102**: 10391–10422.

Zhang HP, King B, Swinney HL. 2008. Resonant generation of internal waves on a model continental slope. *Physical Review Letters* **100**: 244504. https://doi.org/10.1103/PhysRevLett.100.244504.

